Deciphering and Controlling Structural and Functional Parameters of the Shells in Vesicle-Templated Polymer Nanocapsules

Sergey A. Dergunov,[†,] Andrew G. Richter, [‡] Mariya D. Kim, [†] Sai Venkatesh Pingali,[§] Volker S. Urban, [§] Eugene Pinkhassik[†,*]*

[†]Department of Chemistry, University of Connecticut, 55 North Eagleville Rd, Storrs, CT 06269-3060, USA, [‡]Department of Physics and Astronomy, Valparaiso University, Valparaiso, IN 46383, USA; [§]Center for Structural Molecular Biology, Oak Ridge National Laboratory, P.O. Box 2008 MS-6430, Oak Ridge, TN 37831-6430, USA,

ABSTRACT. Vesicle-templated nanocapsules are prepared by polymerization of hydrophobic acrylic monomers and crosslinkers in the hydrophobic interior of self-assembled bilayers. Understanding the mechanism of capsule formation and the influence of synthetic parameters on the structural features and functional performance of nanocapsules is critical for the rational design of functional nanodevices, an emerging trend of application of the nanocapsule platform. This study investigated the relationship between basic parameters of the formulation and synthesis of nanocapsules and structural and functional characteristics of the resulting structures. Variations in the monomer/surfactant ratio, temperature of polymerization, and the molar fraction of the free-radical initiators were investigated with a multipronged approach, including

shell thickness measurements using small-angle neutron scattering, evaluation of the structural integrity of nanocapsules with scanning electron microscopy, and determination of the retention of entrapped molecules using absorbance and fluorescence spectroscopy. Surprisingly, the thickness of the shells did not correlate with the monomer/surfactant ratio, supporting the hypothesis of substantial stabilization of the surfactant bilayer with loaded monomers. Decreasing the temperature of polymerization had no effect on the spherical structure of nanocapsules but resulted in progressively lower retention of entrapped molecules, suggesting that a spherical skeleton of nanocapsule forms rapidly, followed by filling the gaps to create the structure without pinholes. Lower content of initiators resulted in slower reactions, outlining the baseline conditions for practical synthetic protocols. Taken together, these findings provide insights into the formation of nanocapsules and offer methods for controlling the properties of nanocapsules in viable synthetic methods.

Introduction

Vesicle-templated polymer nanocapsules with controlled permeability of the shells have emerged as a viable platform for nanoreactors, nanosensors, and containers for the delivery of drugs and imaging agents.[1-13] Broad utility of nanocapsules in diverse applications highlights the significance of the development of nanocapsules as a platform technology.[1, 14-15] Furthermore, these applications emphasize the importance of fine-tuning the structural parameters. We and others reported basic characterization of nanocapsules[3, 16-24] but a detailed understanding of the structure and structure/property relationships is far from complete.[25-26] In part, scarcity of detailed information on the structure of nanocapsule shells has been caused by difficulties with obtaining detailed structural information of freestanding polymer shells on the sub-nanometer scale.

Our recent study on the measurement of the shell thickness using small-angle neutron scattering (SANS) not only determined the single-nanometer thickness of the shells but also established a methodology for accurate measurements of thickness of free-standing shells.[16] For example, we found the thickness of polystyrene nanocapsules suspended in benzene to be 1.0±0.1 nm, which agrees well with calculations based on the measured distribution of monomers within the template bilayer.[27] The extreme thinness of the shell makes detection and identification of the thickness signature difficult, but we now have an understanding of SANS signature. Furthermore, we were able to measure the increase of the measured thickness due to coating with surfactant, which enables accurate subtraction to determine the thickness of the polymer shells alone in samples that are stabilized with surfactants, something previous studies were unable to do.[28-30] We have exploited these methods to investigate the relationship between the structure of bilayer-templated nanocapsules and their functional performance. A combination of SANS along with other methods allowed us to set the goals for this study.

Multiple recent studies showed that understanding detailed structural information provided critical insights into controlling the function of nanoscale materials, including nanoparticles, metal-organic frameworks, layer-by-layer films, and self-assembled monolayers.[31-40]

This study focuses on investigating the relationship between basic parameters of the formulation and synthesis of nanocapsules and their structural and functional characteristics. Specifically, we focused on acrylic building blocks and investigated variations in the monomer to surfactant ratio, temperature of polymerization, and the monomer to initiator ratio. These are the most fundamental parameters in customizing the synthesis of nanocapsules using the vesicle-templating method. To place this work in the context of previous studies, we used a mixture of *tert*-butylmethacrylate, butylmethacrylate, and buthylene glycol dimethacrylate that have been used to form nanocapsules. Likewise, we continued using a mixture of sodium dodecylbenzenesulfonate and cetyltrimethylammonium tosylate as surfactants that indicated the formation of stabilized vesicles loaded with monomers. In our previous studies, particularly using the diffusion loading technique, where monomers are allowed to diffuse into the bilayer interior through water, lipid bilayers exhibited a specific capacity for accommodating monomers.[18, 27, 41] Intriguingly, this capacity was not dependent on the structure or nature of the monomers. Accordingly, there was a limited range of monomer/surfactant ratios in the synthesis of nanocapsules, which highlighted the need to investigate the relationship between the formulation of the monomer-loaded bilayer and the structure and performance of the resulting nanocapsules. Here we varied the range of monomer/surfactant ratios from the values indicative of maximal loading capacity of bilayers down to the amount that would correspond to a single contiguous layer of monomer molecules within the bilayer. The temperature of polymerization is the most critical parameter in optimizing the conditions for the synthesis of nanocapsules from the vesicle-monomer assembly. We examined the most practical range of temperatures for the synthesis of nanocapsules. At temperatures higher than 60 ºC, monomers may partially evaporate before the completion of the polymerization. Since the synthesis is done in water, temperatures close to the freezing point constitute a lower limit on the reaction conditions. Finally, the monomer/initiator ratio is an important parameter that might potentially affect the structure and function of bilayer-templated materials. If the fraction of the initiator is too high, one may expect the formation of shorter-chained polymers within the bilayer. However, since we use a high

degree of crosslinking, it is difficult to predict whether shortening of crosslinked chains would negatively affect structural stability or functional performance of nanocapsules. On the other hand, if the amount of the initiator is too low, the polymerization process could become too slow or terminate prematurely before the nanocapsules are fully formed.

The influence of variations in the synthesis parameters on the performance of nanocapsules was investigated with a multipronged approach. We measured the thickness of shells with SANS, obtained SEM images of polymethacrylate nanocapsules after the synthesis, and measured the amount of entrapped and retained molecules using absorbance and fluorescence spectroscopy.

Results and Discussion

Vesicle-templated assembly of nanocapsules. We used the directed assembly method outlined in Figure 1 and described in more detail in previous publications.[17, 42-43] Briefly, we prepared vesicles with monomers (mixture of butyl methacrylate (BMA) and tert-butyl methacrylate (t-BMA), crosslinker (1,4-butanediol dimethacrylate (BGDMA), and initiators (lauroyl peroxide (LP) in pair with 4,4'-Methylenebis(N,N-dimethylaniline) (MDMA)[44] placed into the hydrophobic interior of the bilayers using a concurrent loading approach, where vesicles are formed spontaneously upon hydrating the surfactant/monomer mixture (Figure 1). In these experiments, we used a mixture of an anionic surfactant sodium dodecylbenzenesulfonate (SDBS), and a cationic surfactant cetyltrimethylammonium p-toluenesulfonate (CTAT) to form vesicles. The preparation of vesicles was done in an aqueous solution of Nile Blue A (NBA) dye, used here as a size probe with the smallest dimension of approximately 1 nm. After the polymerization, non-entrapped NBA molecules were removed from the sample. When shells had no pores greater than the size of NBA molecules, the nanocapsules retained NBA molecules entrapped in the aqueous core of the vesicles. In our previous studies, we showed that the mass transfer of molecules through the nanometer-thin shells is fast enough so that all molecules

smaller than the pore size would escape from the capsule within the timescale of our experiments.[3, 17, 20, 42] Therefore, the total amount of retained NBA molecules reflects the yield of nanocapsules without pinhole defects.

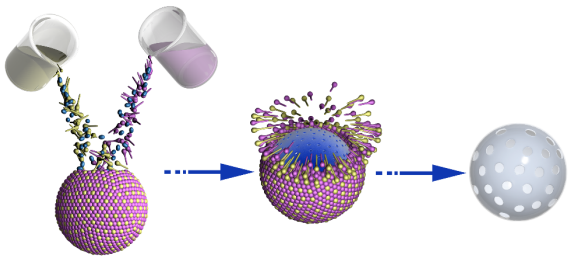

Figure 1. Schematic representation of the synthesis of vesicle-templated nanocapsules: surfactants and monomers are mixed in an aqueous solution producing self-assembled vesicles containing monomers and crosslinkers in the hydrophobic interior of bilayers. Polymerization followed by the removal of the surfactant scaffold yields a suspension of hollow polymer nanocapsules. Shells with the single-nanometer thickness contain small intrinsic pores due to crosslinking of polymer chains. In addition, larger pores can be imprinted in the shells using pore-forming templates during the vesicle assembly and polymerization stages.

In the series of experiments described in detail below, we varied one parameter in the synthesis while keeping the rest of the procedure constant. Specifically, we varied the monomer/surfactant ratio, temperature of polymerization, and monomer/initiator ratio. The thickness of the shells of nanocapsules was measured with the recently published SANS method.[16] We should note that TEM has limited utility in measuring the thickness of nanocapsules at the lower end of the single nanometer range due to curvature of the shells and low contrast of polymer material.[24, 45] We have shown previously the correlation between the thickness of freestanding polymer shell in an organic solvent and the thickness of surfactant-supported shells in water.[16] In these experiments, we showed that the layer of surfactant contributed 2.0 nm to the total thickness of the surfactant-supported shells. Reproducibility of measurements among multiple independently prepared

samples suggested that the thickness of the surfactant layer remained constant under a specific preparation protocol and was reflective of the density of surfactants on the surface of the shells. The contribution to the total thickness due to adsorbed surfactants was in good agreement with literature data reporting the thickness of surfactant layers adsorbed on flat surfaces.[46-48] In the data presented below, however, we chose not to subtract the thickness of the surfactant layer from the total thickness of the surfactant-supported shells so as to minimize processing the results and avoid introducing larger uncertainties.

Table 1. Characteristics ov vesicles after polymerization of monomers. Given are the vesicle deameter D_{ves}, polydispersity index PDI, temperature and time of polymerization, conversion of monomers, measured thickness t_s from the modified Guinier plot.

Sample	D_{ves} (nm)[a]	PDI[a]	T_{pol} (°C)	$Time_{pol}$ (min)	*Conv.* (%)[b]	t_s[c]
NC1	255±3	0.209	40	180	95	ND
NC2	239±5	0.145	40	180	97	3.08
NC3	234±3	0.229	40	190	99	2.81
NC4	230±4	0.304	40	250	95	3.41
NC5	224±3	0.212	40	180	99	2.79
NC6	229±5	0.211	30	220	99	2.66
NC7	234±8	0.229	20	300	88	3.13
NC8	245±7	0.239	5	1200	80	2.81
NC9	249±8	0.185	40	180	99	3.07
NC10	245±5	0.234	40	180	99	2.81
NC11	231±3	0219	40	220	95	2.82
NC12	232±4	0.235	40	300	90	2.83

[a]Monitored using DLS. [b]Measured with GC/MS, [c]Measured with SANS. ND: nondetectable.

Monomer/surfactant ratio. We varied the monomer/surfactant molar ratio from 3:1 to 1:2. Here and below, we say monomer/surfactant for brevity; however, we include monomer, crosslinkers, and initiators in the total amount of building blocks. In terms of accommodating building blocks within the bilayer, these ratios correspond to the values between 6 and 1 monomer molecule(s) sandwiched between two molecules of surfactants that form the bilayer.

Figure 2A shows the SANS curves. Shells should display a characteristic Q^{-2} power-law behavior followed by Porod Q^{-4} scattering; the region where the behavior switches corresponds to the thickness of the shell,[49] which is called the thickness Guinier region. Note that the -2 exponent can vary due to roughness of the surface, porosity of the shell, or the influence of scattering from other length-scales or objects in the sample. Plotting the data as $\ln(IQ^2)$ vs Q^2 gives a modified Guinier plot, which exhibits a linear region near the thickness Guinier region.[50] The slope of that line corresponds to the thickness of the shell.[16] Here and in the figures below, the thickness values correspond to the total thickness of the shell with adsorbed surfactants. In our recent study, we found that the surfactant contributed 2.0 nm to the total thickness when the samples were prepared using the same protocol as the one used in this work.[16] Uncertainties were estimated from the linear fitting process as detailed in our previous paper[16] and are on the order of 0.1 nm.

The most striking finding was that the thickness of the shells of nanocapsules did not correlate with the monomer ratio in the bilayer. Taking into account the area occupied by surfactant molecules and the molar volume of monomers, a fully formed solid film between the surfactant leaflets would range from 2.4 nm to 0.4 nm in thickness for the monomer ratios studied. This simple calculation does not take into account natural porosity in the crosslinked film and resulting voids as well as molecular-level texture of the film; the presence of voids in the shells would translate into thicker structures than solid films. Experimental data show little variation in thickness as the result of varying the monomer concentration. Sample NC1, the highest monomer ratio sample, did not permit reliable thickness measurement as evident from the corresponding SANS data (Figure 2A), likely due to formation of disorganized polymer material – see below for further discussion. The values for the thickness for the remaining samples (NC2, NC3, NC4,

ratios of 2:1, 1:1, 1:2) show some variation but it was non-monotonic and was almost insignificant (about 20%), though the added surfactant thickness likely suppresses the relative change in the polymer shell thickness alone (which may vary by up to 75%). The nominal thickness found for samples NC2, NC3 and NC4 was very close to the values reported recently for the lipid-templated shells.[16, 18, 27, 43] Subtracting the 2.0 nm contribution from the surfactants mentioned above would produce polymer shell thickness values close to 1 nm for each sample rather than varying thickness values ranging from 2.4 nm to 0.4 nm. Considering that all samples underwent identical synthesis and purification protocols, we believe that varied thickness contributions from surfactants are unlikely to account for this discrepancy.

These findings support the hypothesis put forward in our previous paper[43] that surfactants acting together with monomers form stable vesicles. If the surfactant/monomer aggregate shows particular stability in a narrow range of molar ratios, small variations in the thickness values could be explained by this phenomenon. Additional support for the enhanced stability of monomer/surfactant vesicles came from examining the sizes of vesicles. When vesicles are formed from surfactants in the absence of monomers, their average diameter is typically in the 20-60 nm range. When vesicles are formed in the presence of monomers, the average diameter increases to approx. 200 nm. To find whether this diameter could be changed readily, we extruded monomer-loaded vesicles through membranes with cylindrical pores of 100 nm and 50 nm. The average diameter remained at 200 nm as determined by DLS despite the fact that vesicles were forced through a pore much smaller in diameter than the vesicle. In contrast, vesicles formed from phospholipids changed their diameter according to the size of the pores in the filters. A reasonable explanation to these observations is that surfactant vesicles interconvert readily, which is consistent with previous reports and preparation protocols calling for incubation time for the maturation of vesicles.[51-52] When vesicles contain hydrophobic monomers in the bilayer interior, the most stable structures appear to correspond to vesicles with 200nm diameter and specific content of monomers within the bilayer. Therefore, the capsules formed by the polymerization of these monomers would show little difference in thickness regardless of the

initial amount of monomers used for the preparation of vesicles. These observations parallel earlier findings of limited capacity of lipid bilayers for accommodating a specific volume of monomers regardless of their structure or chemical composition.[27, 41]

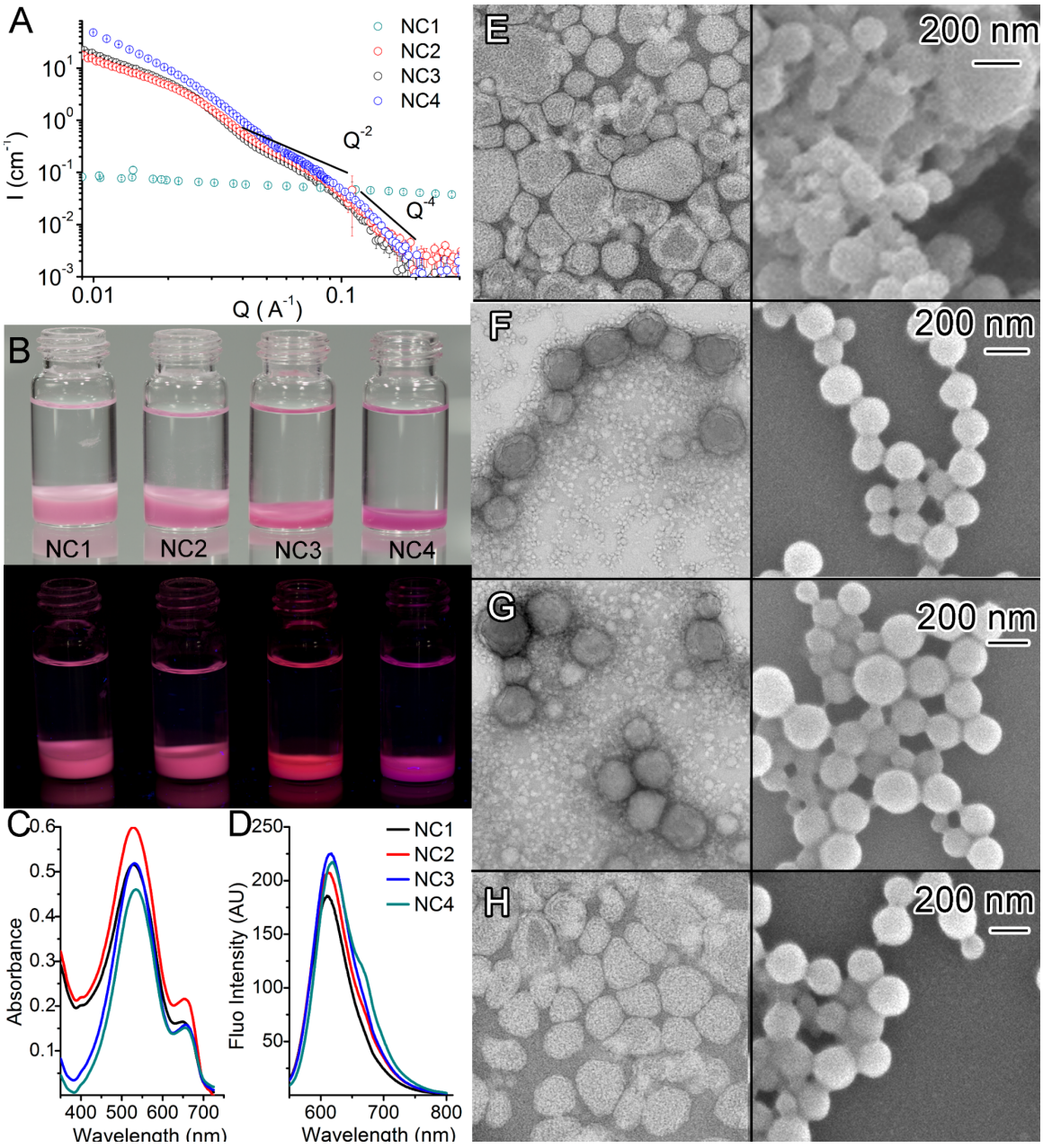

Figure 2. Effects of monomers concentration. (A) SANS curve for nanocapsules stabilized with surfactants and dispersed in D_2O after solvent background subtraction. The lines show the Q^{-2} and Q^{-4} regions for a shell structure. (B) photographs of the corresponding samples (with

incapsulated dye) in methanol under ambient and UV light (bottom); (C) UV-spectra; (D) Steady-state fluorescence emission spectra of entrapped NBA into nanocapsules. Ex.: 530 nm. Spectra ware taken at pH 10.0 in borate buffer with 0.125 wt.% NC. (E-H) TEM and SEM images of nanocapsules synthesised at different concentrations of monomers. Scale bar 200 nm. SDBS:CTAT = 80:20 wt.%, 1% (w/v) solution in water. Ratio initiator to activator = 2:1. Ratio monomers to initiator = 75:1; T=40°C; [monomers] : [surfactants] =3:1 (A-D sample NC1, E), 2:1 (A-D sample NC2, F), 1:1 (A-D sample NC3, G), 1:2 (A-D sample NC4, H)

Retention of entrapped dyes was investigated by absorbance and fluorescence in addition to visual observation (Figure 2B-D). Absolute absorbance values (Figure 2C) appeared higher for samples NC1 and NC2; however, they are clearly skewed by light scattering as evident from apparent increased absorbance at wavelengths below 400nm. Fluorescence data (Figure 2D) suggest that samples NC3 and NC4 retained higher amount of entrapped molecules.

Photographs of samples after polymerization and precipitation with methanol (Figure 2B) corroborate the findings above. In addition, images suggest that samples NC1 and NC2 resulted in a higher yield of polymer material. Combined with retention data, this information implies that samples NC1 and NC2 contain a substantial amount of polymerized material that does not represent fully formed nanocapsules. These conclusions are consistent with the notion discussed above on the mechanism of formation of monomer-loaded vesicles, where surfactant vesicles restructure themselves into the most stable aggregates containing a specific amount of monomers in the bilayer with the remaining monomers aggregating with residual surfactant molecules into monomer-loaded micelles and stabilized emulsions.

Further support for these conclusions comes from TEM and SEM images (Figure 2E-H), particularly from Figure 2E showing sample NC1. This sample clearly shows a large amount of extraneous material in addition to nanocapsules. The SEM image corroborates the finding in SANS experiment (Figure 2A) that showed no discernable features corresponding to shells, consistent with the presence of overlapping signals from random structures on multiple length

scales. The image reveals a few spherical structures larger than 500 nm in diameter. It is likely that these are solid spheres polymerized from stabilized emulsions containing excess monomer. This notion is consistent with lower retention of entrapped molecules observed for sample NC1 compared with samples NC3 and NC4; otherwise one might expect substantially higher retention since larger spheres comprise greater volume than smaller spheres with the same surface area. DLS data did not indicate the presence of larger structures, perhaps due to the relatively small content of these spheres and due to insufficient difference in size to separate light scattering from smaller structures. All samples showed spherical structures with the average diameter matching DLS measurements of vesicles prior to the polymerization from 230 to 255 nm (Table 1). Again, consistency in the formation of nanocapsules with this narrow size range supports the formation of stable monomer-loaded vesicles containing specific amount of monomers associated with the bilayer regardless of the initial surfactant/monomer ratio.

Temperature of polymerization. We conducted the polymerization at four temperatures, 40 °C, 30 °C, 20 °C, and 5 °C. These temperatures cover most of the practical range for the bilayer-templated synthesis of nanocapsules from methacrylic esters monomers used here. Since the vesicles are dispersed in water, the freezing point of water represents a hard lower limit on the temperature. In our experience, incubation of monomer-loaded vesicles at or above 50 °C leads to the noticeable loss of monomers from the bilayers when using monomers with similar volatility to those used in this study. While it is possible to conduct the polymerization at 50 °C or above, the yield of nanocapsules decreases. One should exercise caution with optimizing reaction conditions to ensure that polymerization occurs much faster than the loss of monomers. To avoid complications due to the competition between polymerization and monomer loss, we decided to investigate the synthesis of nanocapsules within the 5-40 °C interval. All four syntheses were performed with the same surfactant/monomer ratio of 1:1 that seemed to be close to the optimal ratio in terms of retention of encapsulated molecules and formation of clean nanocapsules as shown in Figure 2. Polymerization reactions were stopped at the same endpoint. The resulting data are presented on Figure 3.

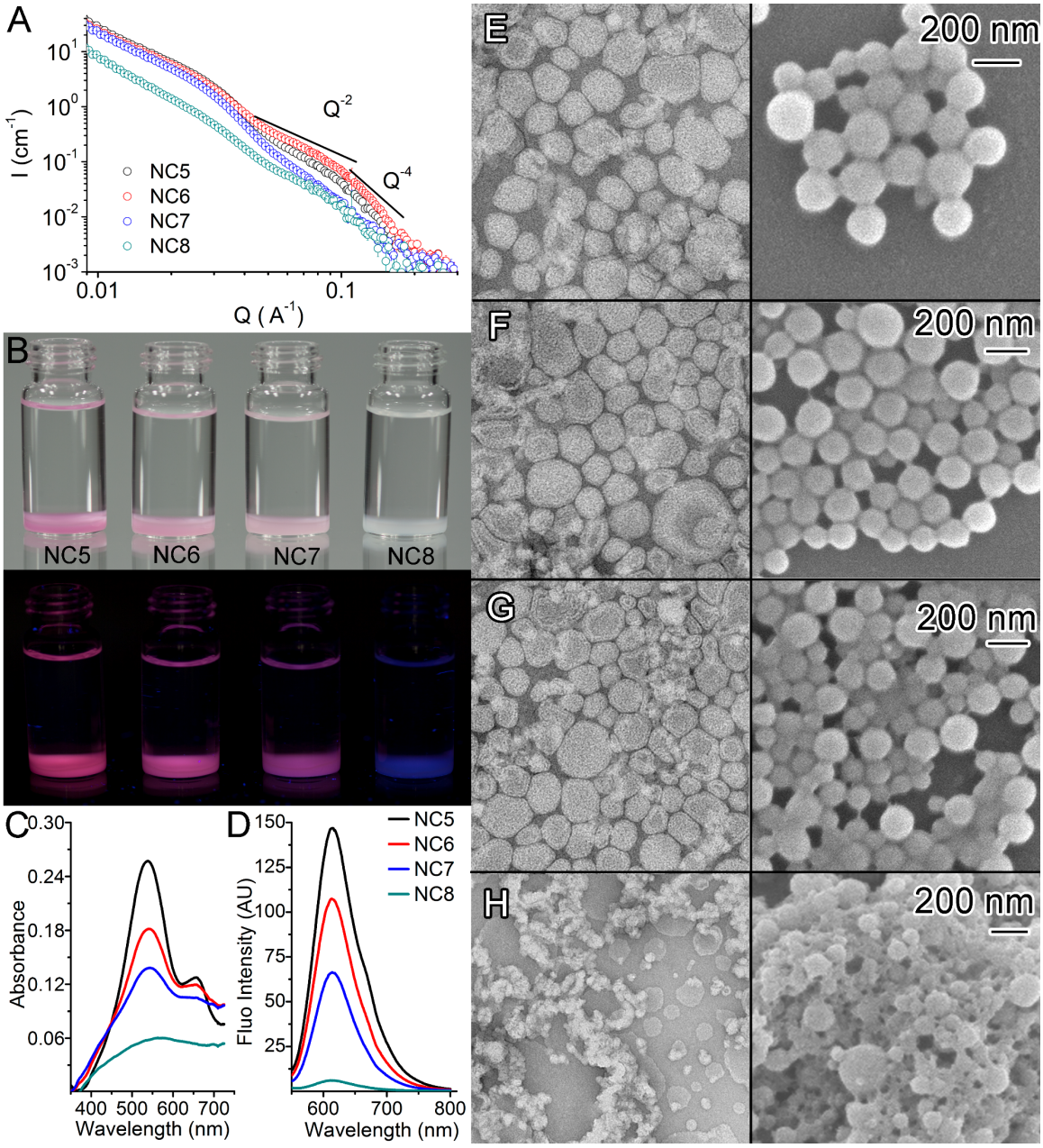

Figure 3. Effects of temperature of synthesis. (A) SANS curve for nanocapsules stabilized with surfactants and dispersed in D_2O after solvent background subtraction. The lines show the Q^{-2} and Q^{-4} regions for a shell structure. (B) photographs of the corresponding samples (with encapsulated dye) in methanol under ambient and UV light (bottom); (C) UV-spectra; (D) Steady-state fluorescence emission spectra of entrapped NBa into nanocapsules. Ex.: 530 nm. Spectra ware taken at pH 10.0 in borate buffer with 0.125 wt.% NC. (E-H) TEM and SEM

images of nanocapsules synthesized at different temperatures. Scale bar 200 nm. SDBS:CTAT = 80:20 wt.%, 1% (w/v) solution in water, [monomers] : [surfactants] =1:1. Ratio initiator to activator = 2:1. Ratio monomers to initiator = 75:1; T=40°C (A-D sample NC5, E), T=30°C (A-D sample NC6, F), T=20°C (A-D sample NC7, G), T=5°C (A-D sample NC8, H)

The most striking difference among the samples was the retention of entrapped molecules. Nanocapsules formed at 40 °C showed the greatest retention by both absorbance and fluorescence measurements corroborated by visual observations (Figure 3B-D). Samples polymerized at lower temperatures showed progressively smaller retention values with the sample produced at 5 °C showing barely any retention of entrapped molecules. Reproducibility of retention data from batch to batch supported systematic differences among the samples.

For samples NC5, NC6, NC7, the yield of polymer material seemed to be comparable judging from the amount of precipitate collected after the synthesis and removal of surfactants and other materials soluble in methanol. Figure 3B illustrates the similarities in the yield of polymer material. The intensities of the thickness feature in the SANS data (Figure 3A), suggest that sample NC6 has the largest number of capsules, followed by samples NC5, NC7, and NC8 with progressively fewer. SEM images for samples NC5 and NC6 show clean nanocapsules. Considering substantial differences in retention of entrapped molecules, we conclude that sample NC6 produced at 30 °C contained a number of nanocapsules with pinhole defects that permitted the release of encapsulated molecules after the synthesis. In our previous experiments, we found the transport rates to be fast enough for complete release expected on the timescale of manipulation with the samples, including precipitation and washing to remove non-entrapped materials. We believe these data indicate that the spherical skeleton of the nanocapsules forms relatively quickly followed by completion of the shell structure that fills the gaps in the spherical polymer network. Samples NC7 and NC8 provide further evidence of this idea since the TEM and SEM of these samples reveals nanocapsules with some extraneous overlaying material (Figure 3G, H). At lower temperatures, the completion of the polymer shells may be too slow to

dominate over other modes of oligomerization, resulting in fewer capsules and more random polymeric material.

The SANS signatures confirm the SEM results (Figure 3A). Scattering from the non-capsule material overlaps with the shell signatures in SANS curves, especially in the case of sample NC7. Sample NC8, the lowest temperature sample, actually shows a slightly more distinct shell signature than sample NC7, which may be the result of the production of smaller oligomers that would not interfere as strongly at the same length-scale as the shell thickness. The lower quality SANS data for samples NC7 and NC8 introduces larger uncertainty in the determination of shell thickness for these samples. Within error, all samples show essentially the same shell thickness (Table 1), further supporting the proposed mechanism for the capsule formation.

Extrapolating the results of temperature-dependent outcomes suggests that increasing the temperature further could result in faster polymerization. As mentioned above, high temperatures could accelerate the loss of monomers from bilayers, which should be taken into account when designing a synthetic protocol. Use of less volatile monomers or minimizing the headspace, particularly in scale-up procedures are likely to lower the losses of monomers potentially allowing for increased temperature of the polymerization.

Monomer/initiator ratio. We varied the monomer/initiator ratio from 60:1 to 480:1 aiming at covering the most practical range based on our preliminary experiments and prior studies with different monomers. The molar fraction of initiators used here was higher than typical fractions of initiators in bulk free-radical polymerization processes.[53-54] The need for higher amounts of initiator is consistent with the polymerization in the two-dimensional confinement of the bilayer where newly formed radicals are exposed to the bilayer leaflets, leading to greater opportunities for termination steps. In general, a higher content of initiator in free-radical polymerization translates into shorter polymer chains.[55-56] In these experiments, we used 1:1 monomer/surfactant ratio and 40 °C as the temperature of polymerization since the studies above suggested that these conditions resulted in more favorable outcomes for the retention of entrapped molecules.

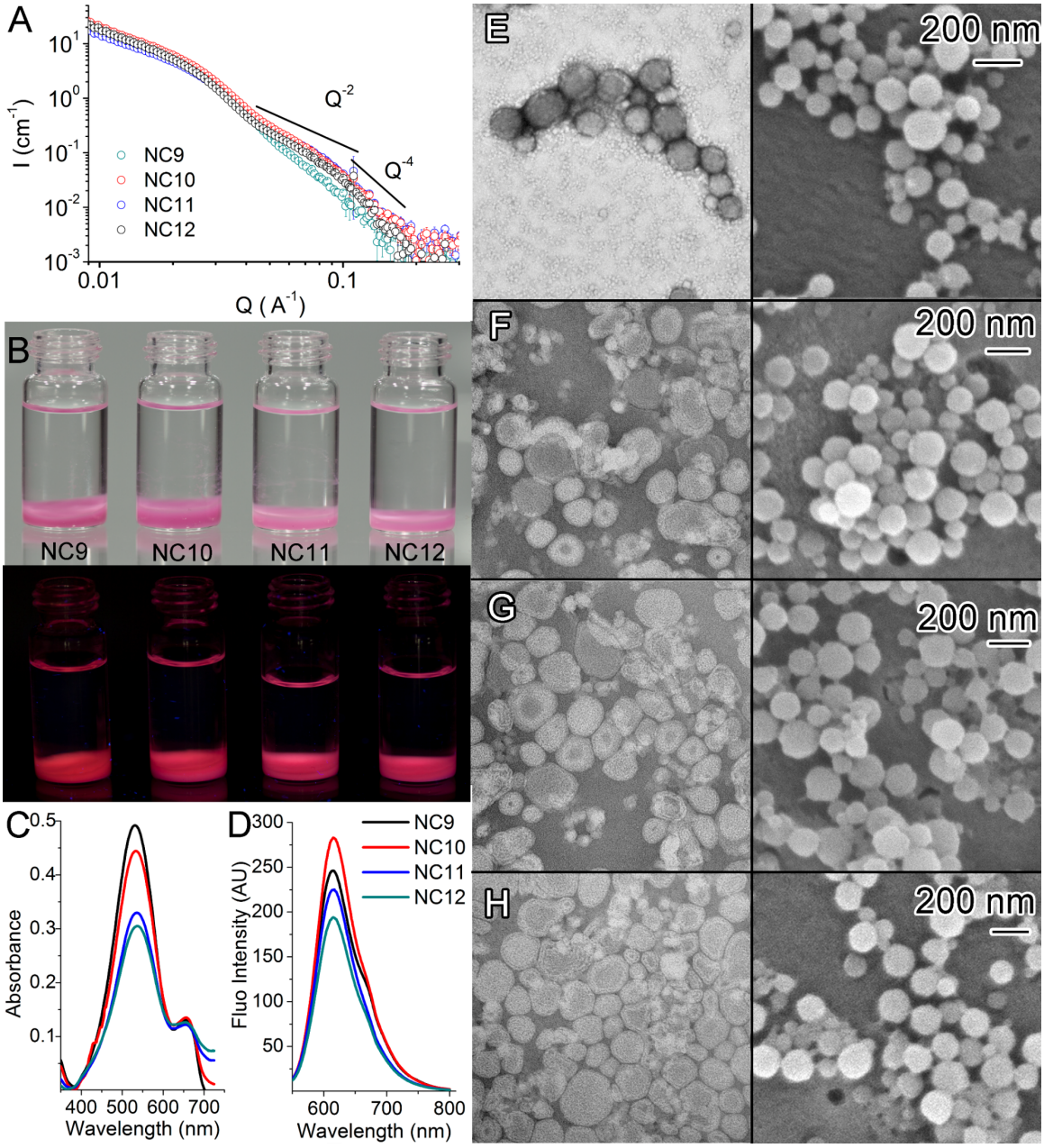

Figure 4. Effects of initiator concentration. (A) SANS curve for nanocapsules stabilized with surfactants and dispersed in D_2O after solvent background subtraction. The lines show the Q^{-2} and Q^{-4} regions for a shell structure. (B) photographs of the corresponding samples (wuth incapsulated dye) in methanol under ambient and UV light (bottom); (C) UV-spectra; (D) Steady-state fluorescence emission spectra of entrapped NBa into nanocapsules. Ex.: 530 nm. Spectra ware taken at pH 10.0 in borate buffer with 0.125 wt.% NC. (K-N) SEM images of

nanocapsules synthesized at different initiator concentrations. Scale bar 200 nm. SDBS:CTAT = 80:20 wt.%, 1% (w/v) solution in water, [monomers] : [surfactants] =1:1. Ratio initiator to activator = 2:1. T=40°C. Ratio monomers to initiator = 60:1 (A-D sample NC9, E), 150:1 (A-D sample NC10, F), 230:1 (A-D sample NC11, G), 480:1 (A-D sample NC12, H)

The highest amount of initiator, sample NC9, resulted in slightly thicker shells (Table 1). This result is consistent with the notion of rapid formation of spherical shell network. Indeed, simultaneous initiation of the polymerization in a greater number of places within the bilayer is more likely to translate into thicker shell due to rapid crosslinking, while slower polymerization is more likely to even out the shell structure within the bilayer. The thicknesses of samples NC10, NC11, NC12 were the same within error, indicating that there may be a minimum threshold of initiator concentration before the crosslinking becomes rapid enough to lead to thicker shells.

Increased content of initiator correlated with increased retention of entrapped molecules judging from absorbance and fluorescence data as well as visual observations (Figure 4B-D). The monomer/initiator ratios explored here produced nanocapsules with noticeably varying retention of entrapped dyes. The highest retention was roughly 50% greater than the lowest retention value.

SEM images (Figure 4E-H) showed virtually identical structures across different monomer/initiator ratios. The average size of nanocapsules was the same as the average size of structures observed in DLS before purification of nanocapsules (Table 1) suggesting no collapse or other structural changes of nanocapsules during the removal of surfactant shell and non-entrapped molecules. Taken together with the data on retention of entrapped molecules (Figure 4B-D) and excellent batch to batch reproducibility, SEM images support rapid formation of the spherical shell followed by completion of the two-dimentional polymer network within the bilayer that removed pinholes in the shell structure. We infer that lower content of initiator

translated to slowed reactions that did not complete the formation of the shell within the experiment time, leading to leakier shells.

Conclusions

The three parameters investigated in this work offered new insights into the mechanism of vesicle-templated assembly of nanocapsules and revealed substantial influence on the resulting structure and function of nanocapsules. The monomer/surfactant ratio affected the yield of clean nanocapsules. Increasing the amount of monomers beyond an optimal ratio of 1:1 offered no benefit for the synthesis of nanocapsules or retention of encapsulated cargo while producing additional non-capsule structures. The combination of neutron scattering, electron microscopy, and dye retention studies supports the hypotheses of stabilization of a bilayer with monomers and the formation of a thermodynamically stable monomer/surfactant aggregate with optimal stability in a narrow range of monomer/surfactant molar ratios.

Variations in the temperature of polymerization suggests that the synthesis of nanocapsules proceeds through the rapid formation of a spherical shell followed by filling the gaps in the shell structure. This finding has implications for the synthesis and application of nanorattles containing large entrapped species, particularly temperature-sensitive materials where rapid shell formation is essential and where retention characteristics are likely to be sufficient even with incomplete walls. Alternatively, one may envision functionalizing the partially formed spherical skeletal network with other monomer/crosslinker combinations, e.g., closing up the capsule with degradable patches that could be removed with an external trigger. The temperature should be as high as feasible to increase the speed of polymerization as long as the loss of monomers from the bilayer is negligible in the timescale of the polymerization.

Changes in the monomer/initiator ratio showed some ability to control the thickness of the shells with the highest proportion of initiator resulting in thicker shells, but also that a wide range

of ratios result in good quality nanocapsules. The molar fractions of initiators were higher than those typically used in the bulk processes, consistent with polymerization in the two-dimensional confinement of a bilayer.

The practical implications of these new insights into the synthesis of nanocapsules include the rational choice of synthesis conditions for maximizing retention of entrapped molecules combined with efficient high-yield synthesis. Combined with previous studies, e.g., observation of specific bilayer capacity irrespective of monomer structure,[57] these data suggest that these findings can be generalized into other vesicle-templating systems. Furthermore, these studies provide a framework for deliberate and efficient optimization of the synthesis procedures with new monomers or crosslinkers, initiators, and amphiphilic scaffolds.

2. EXPERIMENTAL SECTION

Chemicals. Nile Blue A (NBA), Sodium dodecylbenzenesulfonate (SDBS, an anionic surfactant), cetyltrimethylammonium p-toluenesulfonate (CTAT, a cationic surfactant), lauroyl peroxide (LP, an initiator), 4,4'-Methylenebis(N,N-dimethylaniline) (MDMA, an activator) Triton X100 (TX100) and chloroform ($CHCl_3$) were used as received (Sigma-Aldrich). tert-Butyl methacrylate (t-BMA), butyl methacrylate (BMA), 1,4-butanediol dimethacrylate (BGDMA), were purchased from Sigma-Aldrich and were passed through alumina column to remove the inhibitor shortly before sample preparation. Benzene-d_6 (C_6D_6), sodium dodecyl sulfate-d_{25} (SDS-d), deuterium oxide (D_2O) were purchased from Cambridge Isotope Laboratories Inc. and used as received. The solvents and other chemicals used in this study were HPLC and ACS reagent grade, respectively, and were used as received.

Vesicles preparation. To prepare stock solutions, SDBS (100 mg) was mixed with methacrylic ester monomers (1:1:1 mixture of t-BMA, BMA, and BGDMA) and initiator LP. The amounts of monomers and initiator were varied so as to achieve the ratio of monomers to

surfactants between 3:1 and 1:2, and monomers to initiator between 480:1 and 90:1 in the final aqueous solutions after mixing of SDBS and CTAT stock solutions. CTAT (100 mg) was mixed with 1:1:1 mixture of t-BMA, BMA, and BGDMA and activator MDA. The amounts of the monomer mixture and activator were varied as described above. Each mixture was hydrated in 10 mL of deionized water, or dye solutions, or D_2O. CTAT stock solution was equilibrated at temperature 40 °C during 30 min. Samples were prepared by mixing the stock solutions at proper volume ratios after brief vortexing. The mixed solutions were not subjected to any type of further mechanical agitation and were additionally equilibrated at room temperature during 1 hour or were extruded 5 times at 25 °C through a track-etched polyester Nucleopore membrane (Sterlytech) with 0.2 μm pore size using a Lipex stainless steel extruder (Northern Lipids).

Synthesis of nanocapsules. Monomer-loaded vesicles prepared as described above were purged with nitrogen and set to incubate in the thermostated bath at the desired temperature. Kinetics of polymerization of monomers were monitored with GC/MS Shimadzu at temperatures from 60 to 280 °C using 30m SH-RXi-5Sil MS column (Restek), with split ratio 20 at a flow rate of 1 mL min^{-1} (AOC 20i Shimadzu Autoinjector), ion source temperature was 200 °C. Detection was performed using a GCMS QP2010SE Detector operating with MWs from 60 to 700. The system was calibrated with mixture of monomers used in current study. 100 μl of sample was mixed with 3 ml of hexane for extraction of monomers then $NaSO_4$ was added to organic solution. Samples were filtered through a 0.45 μm PTFE filter before analysis.

Following the polymerization, a solution of NaCl (3 drops or approx. 0.02 mL of 3M aqueous solution) in methanol (10 mL) was added to the reaction mixture to precipitate the nanocapsules. The nanocapsules were separated from the reaction mixture and purified by repeated centrifugation (2,000 g for 5 minutes) and resuspension steps using methanol (3 drops of 3M aqueous NaCl were added to aid precipitation), then water-methanol mixture, and finally water as washing solutions.

Samples for SANS analyses were prepared in D_2O in a similar manner to the procedure described above. After the synthesis, TX100 (10 % w/v in D_2O) was added to the suspension of vesicles so as to achieve 3% concentration of TX100 for the dissolution of vesicles and removing surfactant scaffolds from nanocapsules. After that, urea (12 M in D_2O) and NaCl (3 M in D_2O) were added to achieve the total concentration of salt in the mixture equivalent to 1 M. The sample was dialyzed using 100 kDa cellulose tubes against diluted urea solution (0.1 M) for one day and after that against water for a week. Then the sample was concentrated (EMD Millipore™ Amicon™ Ultra-4 Centrifugal Filter Units, 100 kDa) and water was replaced with D_2O in filter units for a week. In all experiments, amounts of all components and solvents were similar.

Small-Angle Neutron Scattering (SANS).

SANS measurements were performed with the CG-3 Bio-SANS instrument at the High Flux Isotope Reactor (HFIR) facility of Oak Ridge National Laboratory and with the NC-7 SANS instrument at the National Institute of Standards and Technology's Center for Neutron Research (NCNR).[58-59] Quartz cells of 2 mm thickness were used to hold the liquid samples. At both facilities, we collected data with $\lambda = 6\,\text{Å}$ ($\Delta\lambda/\lambda \approx 12\%$) using Ordela area detectors. The Q-range, where $Q = (4\pi/\lambda)\sin\theta$ and θ is the scattering angle, was ~0.01 $Å^{-1}$ to ~0.5 $Å^{-1}$. The scattering curves were obtained by azimuthally averaging the processed 2D images, which were normalized to incident beam monitor counts, and corrected for detector dark current, pixel sensitivity and empty beam scattering background.[60] In order to maximize contrast, we used fully hydrogenated monomers to form the nanocapsules which were dispersed in D_2O. To remove background intensity, we multiplied a background D_2O scan by an adjustable parameter and subtracted that modified background data from the sample data, such that the resulting Porod plots, IQ^4 vs Q^4, were flat at high Q.

The shell thickness is found by using a modified Guinier plot, $\ln(IQ^2)$ vs Q^2, in the range where the scattering changes from Q^{-2} to Q^{-4} behavior. The intensity in this region

approximately follows a function $I(Q) \approx A\exp(-Q^2R_t^2)/Q^2$ where $R_t^2 = T^2/12$ and A is a value related to the scattering contrast. Therefore, the modified Guinier plot results in a straight line in that region with a slope of $-R_t^2$, from which we obtain the shell thickness. Because this linear region is bounded by regions that curve and because the intensity is fairly low at these high Q values so that the data is somewhat noisy, the linear fits depend on the choice of starting and ending points for the fits. Therefore, the thickness and its error are estimated by selecting a variety of starting and ending points for the linear fit and finding the average and standard deviation of the resulting values.[16]

Dynamic Light Scattering (DLS). Hydrodynamic diameter and polydispersity index (PDI) measurements were performed on a Malvern Nano-ZS Zetasizer (Malvern Instruments Ltd., Worcestershire, U.K.) equipped with a Helium-Neon laser, 4mW, operated at 633 nm, with the scatter angle fixed at 173°. The temperature was set at 25 °C. 80 μL samples were placed into disposable cuvettes without dilution (70 μL, 8.5 mm center height Brand UV-Cuvette micro). Each data point was an average of 10 scans. Data were processed using non-negative least squares (NNLS) analysis.

Electron microscopy images (SEM and TEM) Transmission electron microscopy images were obtained with a Thermo Fisher Scientific Tecnai 12 G2 Spirit BioTWIN TEM transmission electron microscope (Hillsboro, OR) at a working voltage of 80 kV. To prepare the sample for TEM analysis, a drop of sample was carefully placed on a 200-mesh carbon grid and excess sample was wiped away with filter paper. Then a drop of 2% Uranyl Acetate was added to the grid to negatively stain the sample. After 1 min, the excess liquid was wiped off. To prepare the sample for SEM analysis (Thermo Fisher Teneo LoVac Field Emission SEM (FE-SEM), at a working voltage of 5 kV), a drop of sample was dispersed in 4 ml of pure DI water or benzene and passed through a track-etched polyester Nucleopore membrane (Sterlitech) with 0.2 μm pore size using a Lipex stainless steel extruder (Northern Lipids). Membrane was freeze-dried and placed on SEM pin stub specimen mount covered with double coated carbon

conductive tabs and dried under vacuum. The studied samples were coated with a 7nm gold-palladium (60:40) layer using Polaron E5100 SEM Coating Unit.

Dye retention experiment. A previously described colored size-probe retention assay was used to demonstrate successful formation of nanocapsules.[19-20] Molecules with different colors and sizes were encapsulated in surfactant vesicles, the polymerization was carried out, and nanocapsules were separated from released size probes on a size-exclusion column and/or by precipitation of nanocapsules in methanol and purification by repeated centrifugation and resuspension steps using first methanol (3 drops of 3M NaCl were added to aid precipitation), then water-methanol mixture, and finally pure water as washing solutions. The amount of retained dyes was measured by UV-vis spectroscopy as described below.

Optical spectroscopy. For the absorbance measurements of the dye-loaded nanocapsules, an Olis SM 72 UV-vis spectrophotometer (Bogart, GA) was used in combination with an integrating cavity (Olis CLARiTY sample holder) used here to minimize the interference from light scattering in turbid samples. The CLARiTY accessory was equipped with 8 ml quartz cuvettes containing a "chimney" with an inner diameter of 10 mm. Samples were placed in custom-made quartz test tubes (QSI Quartz scientific inc.) with an outer diameter of 9.8 mm and volumes 2 mL that were inserted into the CLARiTY cuvettes. To ensure reproducibility in measurements, the same test tube was used for all measurements of a series of samples and the test tube was positioned the same way in the CLARiTY cuvette. Steady-state fluorescence spectra were recorded on Cary Eclipse Fluorescence Spectrophotometer (Agilent). The photophysical data (steady-state absorption and fluorescence) of all free and encapsulated dyes were obtained in water and in buffer solutions at different pH values.

AUTHOR INFORMATION

Corresponding Author

*Phone: (1) 860-486-3214. Fax: (1) 860-486-2981. Email: eugene.pinkhassik@uconn.edu, sergey.dergunov@uconn.edu

Notes

The authors declare no competing financial interests.

ACKNOWLEDGMENTS

This work was supported by the National Science Foundation (CHE-1709921, CHE-1522525, CHE-1316680, and CHE-1012951) and the University of Connecticut Research Excellence Program. SEM and TEM studies were performed using the facilities in the UConn/FEI Center for Advanced Microscopy and Materials Analysis (CAMMA). Neutron scattering research conducted at the Bio-SANS instrument, a DOE Office of Science, Office of Biological and Environmental Research resource, used resources at the High Flux Isotope Reactor, a DOE Office of Science, Scientific User Facility operated by the Oak Ridge National Laboratory. We acknowledge the support of the National Institute of Standards and Technology, U.S. Department of Commerce, in providing the neutron research facilities used in this work.

REFERENCES

1. Dergunov, S. A.; Kim, M. D.; Shmakov, S. N.; Pinkhassik, E. Building Functional Nanodevices with Vesicle-Templated Porous Polymer Nanocapsules. *Acc. Chem. Res.* **2019**, *52* (1), 189-198.
2. Dergunov, S. A.; Khabiyev, A. T.; Shmakov, S. N.; Kim, M. D.; Ehterami, N.; Weiss, M. C.; Birman, V. B.; Pinkhassik, E. Encapsulation of Homogeneous Catalysts in Porous Polymer Nanocapsules Produces Fast-Acting Selective Nanoreactors. *ACS Nano* **2016**, *10* (12), 11397-11406.
3. Dergunov, S. A.; Miksa, B.; Ganus, B.; Lindner, E.; Pinkhassik, E. Nanocapsules with ''invisible'' walls. *Chem. Commun.* **2010**, *46*, 1485-1487.
4. Kim, M. D.; Dergunov, S. A.; Lindner, E.; Pinkhassik, E. Dye-Loaded Porous Nanocapsules Immobilized in a Permeable Polyvinyl Alcohol Matrix: A Versatile Optical Sensor Platform. *Anal. Chem.* **2012**, *84* (6), 2695-2701.
5. Miksa, B. Recent progress in designing shell cross-linked polymer capsules for drug delivery. *RSC Advances* **2015**, *5* (107), 87781-87805.
6. Soppimath, K. S.; Aminabhavi, T. M.; Kulkarni, A. R.; Rudzinski, W. E. Biodegradable polymeric nanoparticles as drug delivery devices. *J. Control. Release* **2001**, *70* (1), 1-20.

7. Sun, Q.; Cheng, D.; Yu, X.; Zhang, Z.; Dai, J.; Li, H.; Liang, B.; Shuai, X. A pH-sensitive polymeric nanovesicle based on biodegradable poly(ethylene glycol)-b-poly(2-(diisopropylamino)ethyl aspartate) as a MRI-visible drug delivery system. *J. Mater. Chem.* **2011**, *21* (39), 15316-15326.
8. Tanner, P.; Baumann, P.; Enea, R.; Onaca, O.; Palivan, C.; Meier, W. Polymeric Vesicles: From Drug Carriers to Nanoreactors and Artificial Organelles. *Acc. Chem. Res.* **2011**, *44* (10), 1039-1049.
9. Wang, K.; He, Q.; Yan, X.; Cui, Y.; Qi, W.; Duan, L.; Li, J. Encapsulated photosensitive drugs by biodegradable microcapsules to incapacitate cancer cells. *J. Mater. Chem.* **2007**, *17* (38), 4018-4021.
10. Wang, Y.; Bansal, V.; Zelikin, A. N.; Caruso, F. Templated Synthesis of Single-Component Polymer Capsules and Their Application in Drug Delivery. *Nano Lett.* **2008**, *8* (6), 1741-1745.
11. Musyanovych, A.; Landfester, K. Polymer Micro- and Nanocapsules as Biological Carriers with Multifunctional Properties. *Macromolecular Bioscience* **2014**, *14* (4), 458-477.
12. Sun, H.; Chen, C.-K.; Cui, H.; Cheng, C. Crosslinked polymer nanocapsules. *Polym. Int.* **2016**, *65* (4), 351-361.
13. Larrañaga, A.; Lomora, M.; Sarasua, J. R.; Palivan, C. G.; Pandit, A. Polymer capsules as micro-/nanoreactors for therapeutic applications: Current strategies to control membrane permeability. *Prog. Mater Sci.* **2017**, *90*, 325-357.
14. Sukhorukov, G.; Fery, A.; Möhwald, H. Intelligent micro- and nanocapsules. *Prog. Polym. Sci.* **2005**, *30* (8), 885-897.
15. van Dongen, S. F. M.; de Hoog, H.-P. M.; Peters, R. J. R. W.; Nallani, M.; Nolte, R. J. M.; van Hest, J. C. M. Biohybrid Polymer Capsules. *Chem. Rev.* **2009**, *109* (11), 6212-6274.
16. Richter, A. G.; Dergunov, S. A.; Kim, M. D.; Shmakov, S. N.; Pingali, S. V.; Urban, V. S.; Liu, Y.; Pinkhassik, E. Unraveling the Single-Nanometer Thickness of Shells of Vesicle-Templated Polymer Nanocapsules. *J. Phys. Chem. Lett.* **2017**, *8* (15), 3630-3636.
17. Kim, M. D.; Dergunov, S. A.; Pinkhassik, E. Directed Assembly of Vesicle-Templated Polymer Nanocapsules under Near-Physiological Conditions. *Langmuir* **2015**, *31* (8), 2561-2568.
18. Kim, M. D.; Dergunov, S. A.; Richter, A. G.; Durbin, J.; Shmakov, S. N.; Jia, Y.; Kenbeilova, S.; Orazbekuly, Y.; Kengpeiil, A.; Lindner, E.; Pingali, S. V.; Urban, V. S.; Weigand, S.; Pinkhassik, E. Facile Directed Assembly of Hollow Polymer Nanocapsules within Spontaneously Formed Catanionic Surfactant Vesicles. *Langmuir* **2014**, *30* (24), 7061-7069.
19. Dergunov, S. A.; Kesterson, K.; Li, W.; Wang, Z.; Pinkhassik, E. Synthesis, Characterization, and Long-Term Stability of Hollow Polymer Nanocapsules with Nanometer-Thin Walls. *Macromolecules* **2010**, *43* (18), 7785-7792.
20. Dergunov, S. A.; Pinkhassik, E. Functionalization of Imprinted Nanopores in Nanometer-Thin Organic Materials. *Angew. Chem. Int. Ed.* **2008**, *47* (43), 8264-8267.
21. Meier, W. Polymer nanocapsules. *Chem. Soc. Rev.* **2000**, *29* (5), 295-303.
22. Ruysschaert, T.; Germain, M.; da Silva Gomes, J. F. P.; Fournier, D.; Sukhorukov, G. B.; Meier, W.; Winterhalter, M. Liposome-based nanocapsules. *NanoBioscience, IEEE Transactions on* **2004**, *3* (1), 49-55.
23. Sauer, M.; Streich, D.; Meier, W. pH-Sensitive Nanocontainers. *Adv. Mater.* **2001**, *13* (21), 1649-1651.
24. Moradi, M.-A.; Bomans, P. H. H.; Jackson, A. W.; van Herk, A. M.; Heuts, J. P. A. A quantitative cryoTEM study on crosslinked nanocapsule morphology in RAFT-based vesicle polymerization. *Eur. Polym. J.* **2018**, *108*, 329-336.
25. Baek, K.; Hwang, I.; Roy, I.; Shetty, D.; Kim, K. Self-Assembly of Nanostructured Materials through Irreversible Covalent Bond Formation. *Acc. Chem. Res.* **2015**, *48* (8), 2221-2229.
26. Tong, W.; Gao, C.; Möhwald, H. Manipulating the Properties of Polyelectrolyte Microcapsules by Glutaraldehyde Cross-Linking. *Chem. Mater.* **2005**, *17* (18), 4610-4616.

27. Richter, A. G.; Dergunov, S. A.; Ganus, B.; Thomas, Z.; Pingali, S. V.; Urban, V.; Liu, Y.; Porcar, L.; Pinkhassik, E. Scattering Studies of Hydrophobic Monomers in Liposomal Bilayers: An Expanding Shell Model of Monomer Distribution. *Langmuir* **2011**, *27* (7), 3792-3797.
28. McKelvey, C. A.; Kaler, E. W.; Zasadzinski, J. A.; Coldren, B.; Jung, H. T. Templating hollow polymeric spheres from catanionic equilibrium vesicles: synthesis and characterization. *Langmuir* **2000**, *16*, 8285 – 8290.
29. McKelvey, C. A.; Kaler, E. W. Characterization of nanostructured hollow polymer spheres with small-angle neutron scattering (SANS). *J. Colloid. Interf. Sci.* **2002**, *245*, 68-74.
30. Yalcinkaya, H.; Bressel, K.; Lindner, P.; Gradzielski, M. Controlled formation of vesicles with added styrene and their fixation by polymerization. *J. Colloid Interface Sci.* **2018**, *531*, 672-680.
31. Gagner, J. E.; Qian, X.; Lopez, M. M.; Dordick, J. S.; Siegel, R. W. Effect of gold nanoparticle structure on the conformation and function of adsorbed proteins. *Biomaterials* **2012**, *33* (33), 8503-8516.
32. Tayeb, H. H.; Piantavigna, S.; Howard, C. B.; Nouwens, A.; Mahler, S. M.; Middelberg, A. P. J.; He, L.; Holt, S. A.; Sainsbury, F. Insights into the interfacial structure–function of poly(ethylene glycol)-decorated peptide-stabilised nanoscale emulsions. *Soft Matter* **2017**, *13* (43), 7953-7961.
33. Liu, J.; Shin, Y.; Nie, Z.; Chang, J. H.; Wang, L.-Q.; Fryxell, G. E.; Samuels, W. D.; Exarhos, G. J. Molecular Assembly in Ordered Mesoporosity:□ A New Class of Highly Functional Nanoscale Materials. *The Journal of Physical Chemistry A* **2000**, *104* (36), 8328-8339.
34. Suci, P. A.; Klem, M. T.; Arce, F. T.; Douglas, T.; Young, M. Assembly of Multilayer Films Incorporating a Viral Protein Cage Architecture. *Langmuir* **2006**, *22* (21), 8891-8896.
35. Horcajada, P.; Chalati, T.; Serre, C.; Gillet, B.; Sebrie, C.; Baati, T.; Eubank, J. F.; Heurtaux, D.; Clayette, P.; Kreuz, C.; Chang, J.-S.; Hwang, Y. K.; Marsaud, V.; Bories, P.-N.; Cynober, L.; Gil, S.; Férey, G.; Couvreur, P.; Gref, R. Porous metal–organic-framework nanoscale carriers as a potential platform for drug delivery and imaging. *Nature Materials* **2009**, *9*, 172.
36. Quinn, A.; Such, G. K.; Quinn, J. F.; Caruso, F. Polyelectrolyte Blend Multilayers: A Versatile Route to Engineering Interfaces and Films. *Adv. Funct. Mater.* **2008**, *18* (1), 17-26.
37. Cuomo, F.; Lopez, F.; Miguel, M. G.; Lindman, B. Vesicle-Templated Layer-by-Layer Assembly for the Production of Nanocapsules. *Langmuir* **2010**, *26* (13), 10555-10560.
38. Cuomo, F.; Ceglie, A.; Piludu, M.; Miguel, M. G.; Lindman, B.; Lopez, F. Loading and Protection of Hydrophilic Molecules into Liposome-Templated Polyelectrolyte Nanocapsules. *Langmuir* **2014**, *30* (27), 7993-7999.
39. Lee, S.-M.; Chen, H.; Dettmer, C. M.; O'Halloran, T. V.; Nguyen, S. T. Polymer-Caged Lipsomes:□ A pH-Responsive Delivery System with High Stability. *J. Am. Chem. Soc.* **2007**, *129* (49), 15096-15097.
40. Samanta, A.; Tesch, M.; Keller, U.; Klingauf, J.; Studer, A.; Ravoo, B. J. Fabrication of Hydrophilic Polymer Nanocontainers by Use of Supramolecular Templates. *J. Am. Chem. Soc.* **2015**, *137* (5), 1967-1971.
41. Dergunov, S. A.; Schaub, S. C.; Richter, A.; Pinkhassik, E. Time-Resolved Loading of Monomers into Bilayers with Different Curvature. *Langmuir* **2009**, *26* (9), 6276-6280.
42. Kim, M. D.; Dergunov, S. A.; Pinkhassik, E. Controlling the Encapsulation of Charged Molecules in Vesicle-Templated Nanocontainers through Electrostatic Interactions with the Bilayer Scaffold. *Langmuir* **2017**, *33* (31), 7732-7740.
43. Dergunov, S. A.; Richter, A. G.; Kim, M. D.; Pingali, S. V.; Urban, V. S.; Pinkhassik, E. Synergistic self-assembly of scaffolds and building blocks for directed synthesis of organic nanomaterials. *Chem. Commun.* **2013**, *49* (94), 11026-11028.
44. Wilson, G. O.; Henderson, J. W.; Caruso, M. M.; Blaiszik, B. J.; McIntire, P. J.; Sottos, N. R.; White, S. R.; Moore, J. S. Evaluation of peroxide initiators for radical polymerization-based self-healing applications. *J. Polym. Sci., Part A: Polym. Chem.* **2010**, *48* (12), 2698-2708.

45. Williams, D. B.; Carter, C. B. *Transmission Electron Microscopy. A Textbook for Materials Science*. Springer US: New York, 2009; p LXII-775.
46. Despert, G.; Oberdisse, J. Formation of Micelle-Decorated Colloidal Silica by Adsorption of Nonionic Surfactant. *Langmuir* **2003**, *19* (18), 7604-7610.
47. Edwards, D. A.; Adeel, Z.; Luthy, R. G. Distribution of Nonionic Surfactant and Phenanthrene in a Sediment/Aqueous System. *Environmental Science & Technology* **1994**, *28* (8), 1550-1560.
48. Thakkar, K.; Patel, V.; Ray, D.; Pal, H.; Aswal, V. K.; Bahadur, P. Interaction of imidazolium based ionic liquids with Triton X-100 micelles: investigating the role of the counter ion and chain length. *RSC Advances* **2016**, *6* (43), 36314-36326.
49. Glatter, O.; Kratky, O. *Small Angle X-ray Scattering*. Academic Press: New York, 1982.
50. Brasher, L. L.; Kaler, E. W. A Small-Angle Neutron Scattering (SANS) Contrast Variation Investigation of Aggregate Composition in Catanionic Surfactant Mixtures. *Langmuir* **1996**, *12* (26), 6270-6276.
51. Kaler, E. W.; Herrington, K. L.; Murthy, A. K.; Zasadzinski, J. A. N. Phase behavior and structures of mixtures of anionic and cationic surfactants. *J. Phys. Chem.* **1992**, *96* (16), 6698-6707.
52. Kaler, E. W.; Murthy, A. K.; Rodriguez, B. E.; Zasadzinski, J. A. Spontaneous vesicle formation in aqueous mixtures of single-tailed surfactants. *Science* **1989**, *245* (4924), 1371-1374.
53. Nyhus, A. K.; Hagen, S.; Berge, A. A kinetic study of the polymerization of pure meta-divinylbenzene and pure para-divinylbenzene. *J. Polym. Sci., Part A: Polym. Chem.* **1999**, *37* (16), 3345-3359.
54. Iwasaki, T.; Yoshida, J.-i. Free Radical Polymerization in Microreactors. Significant Improvement in Molecular Weight Distribution Control. *Macromolecules* **2005**, *38* (4), 1159-1163.
55. Ford, W. T.; Nishioka, T.; McCleskey, S. C.; Mourey, T. H.; Kahol, P. Structure and Radical Mechanism of Formation of Copolymers of C60 with Styrene and with Methyl Methacrylate. *Macromolecules* **2000**, *33* (7), 2413-2423.
56. Matyjaszewski, K.; Davis, T. P. *Handbook of Radical Polymerization*. John Wiley & Sons, Inc.: Hoboken, 2002; p xvi-920.
57. Banner, L. T.; Danila, D. C.; Sharpe, K.; Durkin, M.; Clayton, B.; Anderson, B.; Richter, A.; Pinkhassik, E. Controlled Loading of Building Blocks into Temporary Self-Assembled Scaffolds for Directed Assembly of Organic Nanostructures. *Langmuir* **2008**, *24* (20), 11464-11473.
58. Lynn, G. W.; Heller, W.; Urban, V.; Wignall, G. D.; Weiss, K.; Myles, D. A. A. Bio-SANS—A Dedicated Facility for Neutron Structural Biology at Oak Ridge National Laboratory. *Physica B: Condensed Matter* **2006**, *385–386, Part 2*, 880-882.
59. Glinka, C. J.; Barker, J. G.; Hammouda, B.; Krueger, S.; Moyer, J. J.; Orts, W. J. The 30 m Small-Angle Neutron Scattering Instruments at the National Institute of Standards and Technology. *J. Appl. Crystallogr.* **1998**, *31* (3), 430-445.
60. Kline, S. Reduction and analysis of SANS and USANS data using IGOR Pro. *J. Appl. Crystallogr.* **2006**, *39* (6), 895-900.